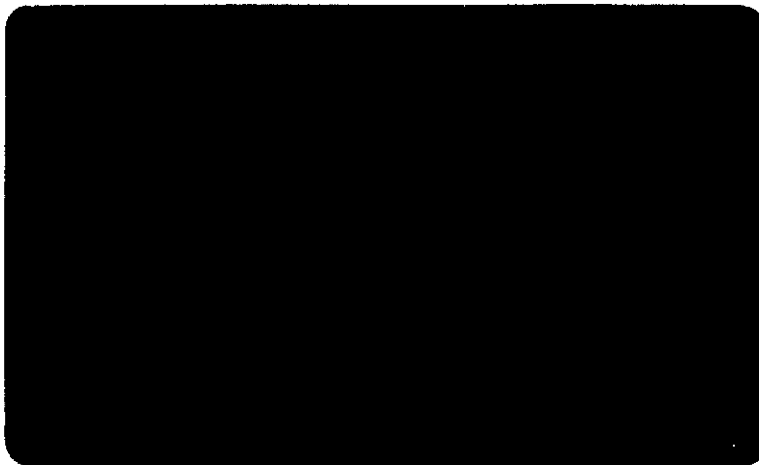


55
2m4

CR 114693



(NASA-CR-114693) MARCH 1971 WIND TUNNEL TESTS OF THE DORAND DH 2011 JET FLAP ROTOR, VOLUME 1 Final Report (Giravions Dorand Co., Suresnes (France)) 55 p HC \$4.75

N74-13722

Unclas
G3/02 26160



GIRAVIONS DORAND

March 1971 Wind Tunnel Tests
of the Dorand DH 2011 Jet Flap Rotor

Final Report

Document DH 2011-D E5 Volume I

June 1973

Contract N° NAS2 - 3673
Modification N° 15 Task C

Prepared by :

Marcel KRETZ
Chief Engineer

Jean-Noël AUBRUN
Research Engineer

Marc LARCHE
Research Engineer

The work reported in this document has been made possible through support and sponsorship of the United States Government through its National Aeronautics and Space Administration, Ames Research Center, in joint participation with U. S. Army Air Mobility Laboratory.

GIRAVIONS DORAND

5, Rue Jean Macé - 92153 SURESNES
FRANCE

Tél. : 772-18-20

/

JUNE 1973ABSTRACT

The results of the March 1971 wind tunnel tests, second series of tests performed in the NASA Ames 40 x 80 foot wind tunnel, of the DH 2011 jet-flap rotor are presented and analysed. The tests have been focused on multicyclic effects and the capability of this rotor to reduce the vibratory loads and stresses in the blades.

The reductions of the vibrations and stresses at tip speed ratio of 0.4 have attained 50%. The theory shows further reductions possible, reaching 80%. The results show that the performance characteristics after the modifications introduced since 1965 remained unchanged. The domain of investigation has been enlarged to include the tip speed ratios of 0.6 and 0.7.

To analyze the complex aeroelastic phenomena a new analytical technique has been utilized to represent the mathematical model of the rotor. This technique, based on transfer matrices and transfer functions, appears very simple and it is believed that this analysis is applicable to many kinds of investigations involving large numbers of variables.

March 1971 Wind Tunnel Tests
of the Dorand DH 2011 Jet-Flap Rotor

Final Report

TABLE OF CONTENTS

	Page
INTRODUCTION	4
SECTION A <u>PRIMARY TEST DATA</u>	7
I Test Configuration Parameter Tables	7
II Rotor Aerodynamic and Performance Coefficient Tables	8
III Performance Coefficients Plots	9
IV Multicyclic Cams Definition and Representation.	10
SECTION B <u>ANALYSIS OF THE RESULTS</u>	13
I Stress and Vibratory Force Data	13
II Analysis of the Multicyclic Effects	15
1. Introduction	15
2. Preliminary investigations	19
3. A general method for studying the rotor .	23
4. Improvements and extension of the method	23
5. Computer program for T matrix identifica- tion and optimal cam evaluation	31
III Application to the Test Data	34
1. Jet flap deflection Fourier analysis	34
2. Analysis of the flap bending stress	35
3. Correction of phase errors ..	35
4. Final results for jet flap deflection and flap bending stress	36

	Page
5. Analysis of the vibrations	40
6. Analysis of the aerodynamic coefficients ..	43
SECTION C <u>CONCLUSIONS</u>	46
1. Data processing	47
2. Vibratory stress analysis	47
3. Vibratory forces	48
4. Performance and aerodynamic aspects of the rotor	49
5. Final remarks	50
REFERENCES	51
APPENDIX I	52

Remark : Tables and figures are presented in volume II

March 1971 Wind Tunnel Tests
of the Dorand DH 2011 Jet Flap rotor

Final Report

INTRODUCTION

The experimental studies concerning the DH 2011 jet flap rotor have started in 1964 by a series of whirl tests outside tunnel (Ref. 1). The first series of wind tunnel tests took place in 1965 in the NASA, Ames 40 - by 80 - foot wind tunnel (Ref. 2 and 5). The second series of wind tunnel test which related in the present report has been preceded by static tests (Ref. 3 and 6).

The application of the jet flap to helicopter rotor blades has been analytically treated in Ref. 4. The practical aspects of the use of jet flap rotors to rotary wing aircraft has been investigated in Ref. 7.

The results of the tests performed in 1965 in the 40 x 80 foot Ames Wind Tunnel have showed the very high lift and high forward speed potential for this type of rotor. Advance ratios up to 0.5 were reached without indications of re-treating blade stall, and the blade loadings exceeded conventional rotor capabilities by factors of 2 and more (Ref. 5). Upon completion of the 1965 tests, it was decided to increase the range of jet deflections and to modify the flap control linkages so that further investigations could be made into the multicyclic potential for relieving vibratory loads and stresses. In fact the DH 2011 rotor possesses the unique feature of introduction of multicyclic control effects by use of mechanical cams acting on the jet flap deflectors, and the exploration of this capability became the main theme of experimental investigation.

This document presents also the analytical technique developed specifically to examine the wind-tunnel results, Ref. 6. In fact the multicyclic effects involve a large number of variables (harmonic components of stresses, loads, control signals) which require special approach to obtain a clear picture of the phenomena studied. As shown later, the technique used is based on transfer matrices and transfer functions and is believed to be more generally applicable to analyze mathematically complex models.

The DH 2011, a full scale 40 ft in diameter, 4.5% solidity, two bladed rotor has been fully described in Ref. 1 through 6. The modifications that have been introduced since the first series of tests in the 40 x 80 Ames Wind Tunnel are three :

1. The pneumatic control system has been replaced by a mechanical one to control with more precision the multicyclic jet flap deflections, which are imposed by predetermined cams.
2. The amplitude of jet flap deflections has been increased from $\pm 25^\circ$ to $\pm 50^\circ$. This increase has been motivated by desire of higher efficiency of jet flap in translational rotor configurations at high advance ratios.
3. The nozzle height has been increased from 4.2 mm to 5.3 to obtain somewhat higher power input and also to be able to judge the influence of the nozzle height on the general performance of the rotor.

The initial test program, Ref. 8, has been performed to a high degree, roughly speaking to 80%. Two main reasons imposed the curtailing of the program, limited to three weeks in the wind tunnel :

1. Lack of power of the air generator, whose pressure ratio was limited to 3.6 (most of the tests have been done at 3.4), the highest pressure ratio expected being 4.0 to 4.2.
2. Premature wear of the mechanical control system that rendered the test procedure more complicated.

During these tests, the rotor has been running a total of 24 hours and 30 minutes, representing 299 measurement points distributed over 29 runs.

An additional run was made to determine the hub drag.

One of the main interest of these tests has been to make possible the study of the effects of a multicyclic control on a jet flap rotor. Numerous measurement points have been made for advance ratios between 0.25 and 0.7. Two values of the blade pitch angle have been tried : $\theta_{0.7} = 5^\circ$ and 3° . A pronounced influence of the multicyclic control has been observed on blade stresses and hub vibratory forces, preliminary investigations showing stress reductions of about 50%.

The test program included originally an optimization of α_g . Unfortunately only few points have been obtained due to limitations in the controls amplitude and it does not seem that they will be enough for the intended purpose.

Aside these tunnel tests, simulations of the multicyclic control have been run in cooperation with NASA research team, on the Ames IBM 360 digital computer.

Dynamic data have been recorded, part by the GIRAVIONS DORAND team, as oscillagraph records, part by the Ames team, as oscillograph and magnetic tape records. Also static values have been read out from the instruments and written down by both teams. These values are presented in Section A in two sets of tables. The first set corresponds to direct readings. The second set to quantities computed from read values by the Ames program FSAO 230.

Despite the fact that it had not been possible to obtain all the planned measurement points the March 71 DH 2011 wind tunnel tests should bring to light many important informations about jet flap helicopter rotors and the efficiency of introduction of a multicyclic deflection law for reducing blade stresses or/and hub vibrations.

PRIMARY TEST DATA

1. TEST CONFIGURATION PARAMETER TABLES (Table I)

In these tables are given the values of the parameters defining the conditions of the test at each measurement point. These values come from direct instrument read-outs. Each test case is coded by two numbers, the first is the run number, the second the measurement point. For example the 7th measurement point of run # 4 is denoted by "run 4-7". This convention will be used throughout the report for its convenience. Symbols used are those of Ref. 4. Some are restated below.

The following quantities are given in the tables:

<u>Symbol</u>	<u>Meaning</u>	<u>Units</u>
θ_{07}	Blade pitch angle	degree
ψ_c	Phasing angle of the multicyclic cam	degree
RPM	Rotor rpm	r. p. m.
T	Rotor thrust	lb
α_s	Rotor shaft angle (negative forward)	degree
α_P	Suspension longitudinal tilt	degree
\bar{A}_0	"Collective" flap deflection	% of max. deflection
\bar{A}_1	"Lateral cyclic pitch" flap deflection	"
\bar{B}_1	"Longitudinal cyclic pitch" flap deflection	"
$\delta\psi$	Multicyclic cam amplitude	% of max. amplitude
\mathcal{J}	Flap deflection peak-to-peak amplitude	degree
Δp	Pressure difference across the flowmeter	mbar
P_1	Pressure at the flowmeter input	bar
V	Tunnel velocity	kts

The flap deflection angle is positive downward. Collective and cyclic components are given by :

$$\bar{A}_0 = \bar{A}_1 \cos \psi - \bar{B}_1 \sin \psi$$

Maximum values of the imposed deflections are

$$\begin{aligned} \bar{A}_{0, \max} &= 50^\circ \\ \bar{A}_{1, \max} &= 30^\circ \\ \bar{B}_{1, \max} &= 30^\circ \end{aligned}$$

It should be noted also that 60% amplitude of multicyclic cam (i. e. Azimuth = 60) corresponds to the theoretical cam amplitude (see paragraph IV for the cams definition).

II. ROTOR AERODYNAMIC AND PERFORMANCE COEFFICIENT TABLES
(Table II)

Basic parameters have been read out for each test point (see Table i) and some others (such as lift and drag, derived from the balance dynamometers signals) have been obtained by the Ames team. From all these measurements, principal aerodynamic coefficients and performance coefficients have been computed by the Ames team on the IBM 360 using the program named FSA 0230.

These coefficients are given in Table II. They are :

<u>Symbol</u>	<u>Meaning</u>	<u>Units</u>
μ	Advance ratio	
α'	Rotor tilt angle	degree
T	Thrust	lb
W	Air mass flow	lb/s
GHP	Isentropic gas power	hp
ESHP	Equivalent shaft power	hp
CJR/ σ	Rotor jet coefficient	
CLR/ σ	Rotor lift coefficient	
CXR/ σ	Rotor propulsive force coefficient	
Cy/ σ	Lateral force coefficient	
CPE/ σ	Rotor shaft power coefficient	
CPP/CPE	Propulsion efficiency ratio	

REMARKS

1. Jet rotor efficiency

The efficiency η of the jet rotor is defined as the ratio of the available mechanical power on the rotor (ESHP in Table II) to the power delivered by the gas generator (GHP).

$$\eta = \frac{ESHP}{GHP}$$

It depends upon the pressure ratio R_p and the rotor r. p. m. . The pressure ratio is defined here at the flowmeter, i. e., if P_0 is the static pressure in the tunnel :

$$R_p = P_1 / P_0$$

During the tests, R_p varies 1.7 to 3.6 and η is found between 28% and 36%. These low values are due to the duct losses ($K_T \sim 3$) and gas temperature which were high in this experimental rotor. This feature made also difficult to match the power supply to the rotor, and hence, not enough power was available for tests at high advance ratio.

Variation of η with R_p are shown in figure 19 for different values of the rotor r. p. m.

2. Propulsion efficiency ratio

This quantity is the ratio η_P of the power available for translation to the power delivered by the engine (here the gas compressor),

$$\eta_P = \frac{XV}{ESHP}$$

or using reduced power coefficients :

$$\eta_P = \frac{(CPP)}{(CPE)} \quad (\text{see table II})$$

The propulsion efficiency ratio is plotted in figure 20 as a function of the advance ratio μ and the rotor tilt angle α' . For small angles,

$$\alpha' \text{ degree} \sim \frac{180}{\pi} X/L$$

The curves show increasing values of η_P with μ and demonstrate the interest of the jet flap rotor for flying at high forward velocities.

III. PERFORMANCE COEFFICIENTS PLOTS

To summarize the numerical results of Table II, different plottings of the values of the most important coefficients are presented here.

Three coefficients have been considered for different values of $\theta_{0,7}$, μ , α_s , \bar{A}_0 and different cam configurations.

They are :

- C_{LR} / σ (lift coefficient)
- C_{XR} / σ (rotor propulsive force coefficient)
- C_{JR} / σ (rotor jet-momentum coefficient)

- All these coefficients are therefore based on an area of 59.4 sqft (i. e. $0,0488 \pi R^2$) which makes them of the C_{LR}/σ type with $\sigma = 0.0488$)

- Plots of C_{LR} vs C_{JR} and C_{LR} vs C_{XR} are given in figures 1 to 18.

Figures 1 to 8 correspond to a blade pitch angle $\theta_{o,\bar{r}}$ of 5° , each plot is made at a given μ but different α_s . The curves corresponding to $\alpha_s = C_{LR}$ result from a fairing of the data points. The same set of curves was used in figures 1 to 4, while in figures 5 to 8, a global translation along the x axis was introduced in each plot, in an attempt for accounting for the change in $V/\Omega R$.

Figure 9 gathers data points corresponding to two values of μ . However, the points are differentiated according to the value of the collective pitch \bar{A}_o in order to obtain a tentative fairing of the curves $\bar{A}_o = cte$.

The same features are found in fig. 9 to 18, corresponding to $\theta_{o,\bar{r}} = 3^\circ$.

Remarks

=====

The scatter found in the results was to be expected because some other parameters than those mentioned previously had changed from one run to another, like for instance the main controls ($\bar{A}_o, \bar{A}_1, \bar{\theta}_1$) and the multicyclic controls. This problem is studied in more detailed in Section C, III.

Nethertheless, the general aspect of the performances is in good agreement with previous tests of the rotor.

The average lift coefficient

$$\bar{C}_L = 6 C_T / \sigma \sim 6 (C_{LR} / \sigma)$$

has reached values above 1, which is characteristic of jet flap rotors, but not a limit. Higher values would have been obtained with more available power on the engine.

VI. MULTICYCLIC CAMS DEFINITION AND REPRESENTATION

1. Definition of the cams.

A multicyclic cam may be defined by the polar equation of its section,

or more conveniently by its Fourier expansion. For a given blade azimuthal angle Ψ , the flap deflection law mechanically imposed by the cam, assuming a perfect transmission, is written as :

$$\mathcal{J}_c = -1,66 A_{\gamma_0} (\bar{A}_2 \cos 2(\Psi + \varphi_c) + \bar{B}_2 \sin 2(\Psi + \varphi_c) + \bar{A}_3 \cos 3(\Psi + \varphi_c) + \bar{B}_1 \sin(\Psi + \varphi_c) + \dots \text{etc})$$

(By convention, \mathcal{J} is positive for flap down)
where φ_c is the angular position of the cam with respect to a fixed reference on the hub, and A_{γ_0} the amplitude of the control (denoted as "Azimuth" in Table I).

For $\varphi_c = 0$ and $A_{\gamma_0} = 60\%$, $\bar{A}_2, \bar{B}_1, \dots$ etc. are the Fourier coefficient of the theoretical multicyclic flap deflection.

- Four cams have been used in the tests. They are denoted as Cams I, III, IV and V, and the corresponding values of \bar{A}_n and \bar{B}_n are given in Table III.
- In general, for given values of A_{γ_0} and φ_c , the Fourier coefficients of the multicyclic law, defined by :

$$\mathcal{J}_c = \mathcal{J}_2 \cos 2\Psi + \mathcal{J}'_2 \sin 2\Psi + \mathcal{J}_3 \cos 3\Psi + \mathcal{J}'_3 \sin 3\Psi + \dots \text{etc}$$

are related to the \bar{A}_n and \bar{B}_n by :

$$\begin{cases} \mathcal{J}_n = -1,66 A_{\gamma_0} (\bar{A}_n \cos n\varphi_c + \bar{B}_n \sin n\varphi_c) \\ \mathcal{J}'_n = -1,66 A_{\gamma_0} (\bar{B}_n \cos n\varphi_c - \bar{A}_n \sin n\varphi_c) \end{cases}$$

2. Graphical representation of the cams

It is convenient to represent graphically a given cam by vectors indicating, for each harmonic, the positions of the blade where the maximum flap deflection occurs when only driven by this harmonic.

This of course will give two opposite vectors for the 2p harmonic, three vectors 120° apart for the 3p, four at 90° for the 4p, and so on.

A change φ_c in the phase setting of the cam will only rotate the whole pattern by an angle φ_c .

In addition, the length of the representative vectors may be made proportional to the corresponding harmonic amplitude.

On figures 21, 22, 23 and 24 are shown this representation of the four cams at $\varphi_c = 0$.

The range of the angles swept by the different harmonics of the four cams used during the tests are shown on figures 23, 24 and 25.

The numerical values of the multicyclic components, $\delta\psi$, of the jet-flap deflection, δ , of five original cams at their 60% control position are given below :

$$\text{Cam I} : \delta\psi = +11 \cos 2\psi$$

$$\text{Cam II} : \delta\psi = +8.4 \cos 2\psi - 1.8 \cos 3\psi + 1.3 \sin 2\psi + 4.5 \sin 3\psi$$

$$\text{Cam III} : \delta\psi = 2.5 \cos 2\psi - 3.5 \cos 3\psi + 2.5 \cos 4\psi + 2.3 \sin 2\psi \\ + 3 \sin 3\psi$$

$$\text{Cam IV} : \delta\psi = 2.5 \cos 2\psi - 3.5 \cos 3\psi + 2.5 \cos 4\psi + 2 \sin 2\psi \\ - 4.0 \sin 3\psi$$

$$\text{Cam V} : \delta\psi = 7.0 \cos 3\psi$$

The components of $\delta\psi$ are given in degrees. Only four cams have been used during tests. The cam N° II has never been used.

ANALYSIS OF THE RESULTS

I. - STRESS AND VIBRATORY FORCE DATA

During the March 71 wind tunnel test of the DH 2011 jet flap rotor, different rotor configurations have been studied with different multicyclic cams. For each cam, several phase settings were used and for a given phase setting, the amplitude of the cam was varied (see Table I and Section B, IV).

The oscillograph records taken then, have been analysed at GIRAVIONS DORAND to determine the effect of the multicyclic cams. Peak-to-peak values of the stresses and vibrations have been measured and compared and these results are displayed in the following tables.

1. - TABLE IV - STRESS REDUCTION (pages 49 to 52)

This table gives the peak-to-peak values of the flap bending stresses at 0.45 and 0.7 R. They are denoted respectively as "ampl. max 4.2/1" and "ampl. max 4.3/1".

The column "CAM. AMPL. %" indicates the percentage of total multicyclic cam amplitude which was used in the corresponding test point.

The stress reduction is given in % according to the formula :

$$\Delta\sigma / \sigma = 100 \frac{\sigma_1 - \sigma_2}{\sigma_1}$$

where σ_1 denotes the value of the stress for zero or small cam amplitude, σ_2 to an increased value of the amplitude. (Therefore, a positive value of $\Delta\sigma / \sigma$ corresponds to a reduction).

Most significant cases exhibiting the stress reducing effect of the multicyclic cams are plotted in figure 38.

The run number corresponding to the value σ_2 is shown on the X axis, and the cam type and phase shift used in this case are indicated right below.

2. - TABLE V - VIBRATORY FORCES REDUCTION (pages 53 to 57)

Peak-to-peak values of the vibratory forces have been measured from the oscillograph records, corresponding to the left vertical arm of the balance (load cell F 5.1).

Conventions for the reduction are the same as for the stresses and a similar display of significant cases is given on figure 39.

Also on figures 28 to 37 are plotted the peak-to-peak values of the vibratory forces as a function of the cam amplitude (figures 28 to 30 contain in addition results for F 5.2 and F 5.3 load cells giving forces in the right aft and forward vertical arm of the balance).

3. - STATISTICAL RESULTS

Several multicyclic cam settings have been tested in an almost random sweep in order to cover as large as possible the available phase-amplitude range for the multicyclic flap deflection (see Section B, IV).

Results of these tests, summarized in table VI below, show that a significant reduction has been obtained in about half of the cases. Similar results are obtained for the vibrations.

	Stresses at		Aft load
	r=0.45R T _{0.45}	r=0.7R T _{0.7}	cell F _{5.1}
More than 5% reduction	26	30	46
More than 5% augmentation	28	24	13
Less than 5% change	12	12	10
Total number of cases	66	66	69

TABLE VI - Statistical effects of the cams

To display the effect of the cams more systematically, statistical effects of the cam phase shift has been studied in the following way :

For a given cam type with a given phase shift, a serie of test points had been made in different flight configuration. In each flight configuration, a first test point was made with no or small

cam amplitude, and the peak-to-peak stress amplitude measured, say σ_1 . For an increased amplitude of the cam, an other test point was made, and the stress was then σ_2 . These two test points constitute a "case" for which the variation of the stress is computed according to Eq. 1. If N cases have been considered for this cam, an averaged variation is computed as :

$$\langle \Delta \sigma / \sigma \rangle = \frac{1}{N} \sum_{i=1}^{i=N} (\Delta \sigma / \sigma)_i$$

This quantity is plotted as a function of the phase shift for each cam on figure 40 for the stresses and figure 41 for the vibrations. This plottings show the marked effect of the phase and therefore the importance of a correct setting for optimum results.

The analysis of the signals has been obtained for different values of δ_v . The results show that stress reductions are non necessarily correlated with reduction of vibratory forces.

Striking examples of stress and vibration reduction obtained by the multicyclic control are displayed on figures 42 to 46. Here are compared the stress (or vibration force) time histories for different multicyclic jet flap deflections, which are also plotted. These signals have been copied from the original oscillograph records taken during the tests.

As it appears, up to 40% reduction of stresses and 48% reduction of vibrations have been observed, which demonstrates clearly that the multicyclic control of the rotor is a powerful means for reducing blade stresses and vibrations.

II. - ANALYSIS OF THE MULTICYCLIC EFFECTS

1. - INTRODUCTION

The overall analysis of the experimental data described in the preceeding paragraph has shown that the multicyclic cams have a definite effect upon the stresses and vibrations. Due to simultaneous variations in other parameters, this analysis has principally a statistical value, but is not sufficient for relating precisely the stress variations to specific properties of the cams. A search for a correlation between stresses and flap deflection has been motivated by three important factors :

- a) the need to establish the actual contribution of the cam and the influence of the other parameters,
- b) the application of such results to the definition of the best type of cam to be used for a systematic stress reduction,

c) the possibility of describing this correlation by a linear transformation as demonstrated on simulated results (Ref. 3).

Indeed, not only μ , α_s and $\theta_{0.7}$ were varied during the tests, but, even for a given flight configuration, the introduction of multicyclic cams was accompanied by some changes in the three main controls \bar{A}_0 , \bar{A}_1 and \bar{B}_1 . Therefore, the first step is to isolate the multicyclic effects and correlate them with the multicyclic components of the cams.

Then the optimization of the cams can be approached in two different ways. One is to simulate as well as possible the rotor dynamics on a computer and try different types of cams, as this was done in the present test. But in this case, the parameters can be set exactly as desired and it is possible to bring out the multicyclic effects only. This has been done at the AMES Research Center using the Evans - Mc Cloud program (Ref. 4). For instance, let us consider a serie of ten simulations corresponding to the following conditions.

$$\begin{array}{lll} \theta_{0.7} = 5^\circ & \alpha_s = - 6^\circ & \\ 250 \text{ r. p. m.} & \mu = 0.25 & \\ C_{JR} = 5.4 \cdot 10^{-4} & C_{LR}/\sigma = 0.096 & C_{xR}/\sigma = 0.007 \end{array}$$

Collective pitch	51.1 degrees	
Cyclic (\bar{A}_1)	0	"
Cyclic (\bar{B}_1)	14.5	"

The program evaluates the Fourier coefficient of the thrust coefficient, C_T , which is more or less representative of the vibratory forces at the hub. One can then deduce the time history and the peak-to-peak values and obtain such table as below :

RUN	CAM COMPONENTS (degree)				$C_T \times 10^3$ peak-to-peak
	ρ_2	ρ'_2	ρ_3	ρ'_3	
50- 1	0	0	0	0	1.7
50- 2	0	0	0	0	1.7
50- 3	- 5	0	0	0	1.21
50- 4	0	- 10	0	0	2.04
50- 5	- 5	- 5	0	0	1.24
50- 6	0	0	- 5	0	2.18
50- 7	0	0	0	- 10	1.73
50- 8	0	0	- 5	- 5	2.02
50- 9	- 5	- 10	- 5	0	1.29
50-10	- 20	0	0	- 5	1.86

TABLE VI - Simulated multicyclic effects on vibrations

From this test, it can be deduced that the cam of run 50- 3 is the best, but in fact there is no way to tell whether it can be improved, particularly by adding a 3 p harmonic component. Actually it exists a cam which reduces C_T down to $0.6 \cdot 10^{-3}$, peak-to-peak value, as it will be seen later in paragraph III.5.

The other problem, is the accuracy of the simulation itself. Computations based upon an uniform induced flow field is indeed known to give good results as far as static values and performances are concerned, but disputable ones when higher harmonics are considered.

Since a realistic mathematical model of the rotor would be far too complicated for evaluating the multicyclic effects, a global description of the rotor using its input - output properties has been proposed which turned out to be very powerful for analysing the test data.

The research has been done on the basis of the Fourier analysis since all the tests were performed in the steady state conditions. The original idea, tested first on simulated data, was to relate the

Fourier coefficients of the measured stress to those of the multicyclic cam, by a linear transformation, considering only the harmonics of rank 2 and 3. But with test measurements this method turned out to be unapplicable for the following reasons :

- a) Due to some imperfections of the mechanical linkage, the actual flap deflection, as measured by the Cimatron, was considerably different from the deflection originated at the cam. It became therefore necessary to Fourier analyse the Cimatron signal instead of using directly the theoretical cam Fourier coefficients in the correlation analysis. Comparison between the Fourier coefficients of the multicyclic cams ordered deflections and those of the actual flap deflection are given in Table VII for 30 runs.
- b) For the same reason, runs which were supposed to be performed with the same collective and cyclic were not really so. Since these controls contribute also to the stresses harmonic content, it was thus necessary to include them in the model, with the multicyclic deflections.

With these modifications, partial results were obtained using few runs, and they were encouraging, the dispersion on some coefficients being less than 10%. However it was soon realized that the analysis should at least include the 4th harmonic because the study of the Cimatron signals showed that it was of a similar or even greater magnitude than the 3rd harmonic. At this point, a least square regression method has been introduced and a 80% correlation obtained on 15 test points.

It appeared then that the value of the rotor shaft angle α_s , could also be included in the model in a linear way. With this modification 30 different test points have been correctly represented by the model.

Finally, this linear representation makes possible the computation of a cam which would reduce the stresses. At first an "ideal cam" was defined according to Ref. 3, which makes zero the 2nd, 3rd and 4th harmonic of the stress. But with this particular definition, peak-to-peak values were not always reduced. An other criterion has been used in recent analyses which leads to a systematic reduction in all 30 cases. Ideal cams corresponding to this new criterion are easy to compute and could be used as starting point in a finer optimization algorithm.

For these correlation studies, a general FORTRAN IV program has been established. All the test points analysed were made at the same advance ratio ($\mu \sim 0.4$), but provisions have been made in this program to include the effect of μ in order to cover a very wide range of test conditions.

2. - PRELIMINARY INVESTIGATIONS

2.1. Basic ideas

In Ref. 3 a method is described for correlating the harmonics 2 and 3 of the jet flap deflection to those of the thrust coefficient C_T , or of the moment coefficient M_T . The hypothesis made there is, that for all runs used in the correlation analysis :

- a) The rotor configuration parameters are the same (i. e. Ω , μ , C_{JR} , $\theta_{0.7}$ and α_S),
- b) The rotor controls are the same (i. e. collective and cyclic flap deflection),
- c) The flap deflection does not contain harmonics of rank greater than 3.

The model proposed in this method for describing the rotor may be derived simply from the expression of the local aerodynamic forces on the blade. Within the assumption of small angles (local angle of attack, flapping angle and jet flap deflection angle) the force by unit area at the distance r of the shaft may be expressed as :

$$f_r = \frac{1}{2} \rho (r\Omega + v \sin \psi)^2 \left[\frac{\partial C_z}{\partial \alpha} (\theta + \varphi) + (C_j + S_L \sqrt{C_j}) \delta^2 \right] \quad (1)$$

where

- V is the free stream velocity
- C_j the jet momentum coefficient
- S_L the jet flap efficiency
- θ the local blade pitch angle
- φ is an aerodynamic angle of attack given by

$$\varphi = (V_i + v_e + v_{\beta} \cos \psi - r\dot{\beta}) / (r\Omega + v \sin \psi)$$

with

V_i induced velocity

V_z flow velocity through the rotor ($= V \alpha q$)

β flapping angle

$$\frac{\partial C_z}{\partial \alpha} = \left(\frac{\partial C_z}{\partial \alpha} \right)_{\text{airfoil}} + C_j + S_L \sqrt{C_j}$$

letting

$$\mu = V / r \Omega$$

$$\sigma = 1 + \mu \sin \psi$$

$$\mu_i = V_i / r \Omega$$

$$\bar{C}_j = C_j \sigma^2$$

it comes :

$$F_r / \frac{1}{2} \rho r^2 \Omega^2 = \sigma^2 \frac{\partial C_z}{\partial \alpha} \theta + \sigma \frac{\partial C_z}{\partial \alpha} (\mu_i - \dot{\beta} / \Omega) \quad (2)$$

$$+ \mu \sigma \frac{\partial C_z}{\partial \alpha} (\beta \cos \psi + \alpha q) + (\bar{C}_j + S_L \sqrt{\bar{C}_j} \sigma) \rho$$

On other hand, the flapping equation may be written as :

$$I \Omega^2 \left(\frac{d^2 \beta}{d \psi^2} + \beta \right) = M_T = \int_0^R F_r r b dr \quad (3)$$

where b is the local chord, and I , the inertia of the blade about the hinge axis.

It is assumed that :

- 1) The induced velocity is uniform ($\mu_i = \text{cte}$)
- 2) The flapping equation can be approximated using the average value of the coefficient of $\dot{\beta}$ (appearing in F_r) and neglecting the term in $\mu \beta \cos \psi$.

Then Eq. 3 may be written as :

$$\frac{d^2 \beta}{d \psi^2} + \frac{2}{\Omega T_0} \frac{d \beta}{d \psi} + \beta = M_0 \quad (4)$$

with

$$\frac{2}{\Omega T_0} = \frac{1}{I} \int_0^R \frac{1}{2} \ell \frac{\partial C_Z}{\partial \alpha} r^3 b dr \quad (5)$$

(This equation defines the time constant T_0 of the rotor)

and
$$M_0 = m_0(\psi) + \zeta_j(\psi) \mathcal{J}(\psi) \quad (6)$$

where

$$m_0(\psi) = \int_0^R \left[\omega^2 \frac{\partial C_Z}{\partial \alpha} \theta + \omega \frac{\partial C_Z}{\partial \alpha} (\mu_i + \mu \alpha g) \right] r b dr \quad (7)$$

$$\zeta_j(\psi) = \int_0^R (\bar{c}_j + s_L \sqrt{\bar{c}_j} \omega) r b dr \quad (8)$$

It is deduced that :

- 1) β is obtained from M_0 by an ordinary linear transfer function.
- 2) M_0 results from the multiplication of the flap deflection by a function of ψ .
- 3) The aerodynamic forces may be expressed in the same way, i. e., multiplication by a function of ψ and then filtering by a linear filter.

$$(F_0 + \zeta \mathcal{J}) \xrightarrow{G(\omega)} f_r$$

Quantities associated with the rotor, such as flapping angle, vibratory forces, stresses and so on, which depend only upon the rotor dynamics, may be expressed as functions of the aerodynamic forces by means of ordinary linear transfer functions. Let x be such a quantity, and $x(\omega)$ its Fourier transform, it comes :

$$x(\omega) = \int_0^R G_r(\omega) f_r(\omega) dr \quad (9)$$

- Such a model may be sketched as in figure 47.

For steady state conditions, all functions can be expanded in Fourier series, such as :

$$x = \sum_{n=-\infty}^{+\infty} x_n e^{jn\Omega t}$$

and a general form for x_n is obtained :

$$x_n = (x)_n + g_n \sum_p \zeta_p \mathcal{J}_{n-p} \quad (10)$$

This expression can be in turn transformed in a relation between the sine and cosine coefficients of the Fourier expansions of X and \mathcal{J} :

$$X(\psi) = X_0 + X_1 \cos \psi + X_1' \sin \psi + X_2 \cos 2\psi + X_2' \sin 2\psi + \dots$$

$$\mathcal{J}(\psi) = \mathcal{J}_0 + \mathcal{J}_1 \cos \psi + \mathcal{J}_1' \sin \psi + \mathcal{J}_2 \cos 2\psi + \mathcal{J}_2' \sin 2\psi + \dots$$

constructing the vectors :

$$X = \begin{pmatrix} X_0 \\ X_1 \\ X_1' \\ X_2 \\ X_2' \\ \vdots \end{pmatrix} \quad X_0 = \begin{pmatrix} X_{00} \\ X_{01} \\ X_{01}' \\ X_{02} \\ X_{02}' \\ \vdots \end{pmatrix} \quad \mathcal{J} = \begin{pmatrix} \mathcal{J}_0 \\ \mathcal{J}_1 \\ \mathcal{J}_1' \\ \mathcal{J}_2 \\ \mathcal{J}_2' \\ \vdots \end{pmatrix}$$

it comes finally :

$$X = T \mathcal{J} + X_0 \tag{11}$$

where T is a matrix independant of \mathcal{J} which consequently defines the relationships between \mathcal{J} , the input to the rotor, to X , considered as its output.

When collective and cyclic terms ($\mathcal{J}_0, \mathcal{J}_1, \mathcal{J}_1'$) are constant, a similar relation can be written between the multicyclic components of X and \mathcal{J} :

$$X_M = T_M \mathcal{J}_M + X_{M0} \tag{12}$$

This type of model was used in Ref. In addition, since the quantity \mathcal{Z} in eq. 6 contained no higher harmonics than the third, it was shown that T_M had some symmetry properties and could be written as :

$$T_M = \begin{pmatrix} g_2 & -h_2 & g_{23} & -h_{23} \\ h_2 & g_2 & h_{23} & g_{23} \\ g_{32} & -h_{32} & g_3 & -h_3 \\ h_{32} & g_{32} & h_3 & g_3 \end{pmatrix} \tag{13}$$

2.2 Results obtained with simulated data

In Ref. 3 was described a graphical method for obtaining the coefficients g and h in T_M . This was possible because of the particular choice of the flap deflection components. A general method has been developed later. It identifies all the coefficients of T_M without assuming any symmetry properties (see paragraph 3 below). The simulated runs, whose characteristics have been described previously in the introduction, have been processed by this method and the following matrix has been found, relating the multicyclic part of the thrust coefficient C_T , to that of the flap deflection :

$$C_T = T_M \mathcal{J}_M + C_{T_0}$$

when \mathcal{J} is expressed in degrees :

$$T_M = 10^{-6} \times \begin{vmatrix} 47.2 & 15.6 & - 9.1 & 17.1 \\ - 15.6 & 47.3 & - 13.5 & - 8.0 \\ 7.4 & - 15.2 & 56.9 & 12.5 \\ 13.8 & 7.6 & - 13.4 & 58.1 \end{vmatrix}$$

The symmetry properties found here are in quite good agreement with eq. 13, which is consistent with the fact that the simulation uses an uniform in flow field and that the variations of β are small. The residual lack of symmetry, however, results from the non-linear effects introduced by blade stall, reverse flow region and perturbations due to β . These deviations are of course increasing with the rank of the harmonic which is considered.

3. - A GENERAL METHOD FOR STUDYING THE ROTOR

3.1 Principle

In steady state conditions, all variables of Eq. 2 and 3 may be expanded in Fourier series. The remarkable feature of these equations is that they are linear with respect to the variables $\beta, \mu_i, \mathcal{J}$, but with periodic coefficients. This leads automatically to linear relations between the Fourier coefficients of these variables.

Since the induced velocity can be computed in the vortex theory from the local aerodynamic forces, its Fourier coefficients are

also related linearly to those of f_r . Eliminating f_r between Eq. 2 and 3, will finally lead to linear relations between the coefficients of β , or f_r , and those of \mathcal{J} .

Finally, the Fourier coefficients of a quantity x associated with the rotor can be linearly related to those of \mathcal{J} and Eq. 11 remains valid :

$$x = T\mathcal{J} + x_0$$

But now, symmetry properties are no longer guaranteed.

Except for stall effects, this model should represent the present rotor with a good approximation. The problem now is to identify the coefficients in T and x_0 from the measurements of x and \mathcal{J} obtained during the tests.

Obviously, T depends upon μ , Ω , θ_0 and α_q (or α_s), and x and \mathcal{J} should correspond to constant values of these coefficients.

3.2 Linear least square multiple regression for multicyclic transfer matrix identification

To proceed conveniently with this identification, it is desirable to write Eq. 11 in the more condensed form :

$$x = T\mathcal{J}$$

where the last column of T is in fact the vector x_0 and the last component of \mathcal{J} is equal to 1.

Calling N , the number of Fourier coefficients of \mathcal{J} ($N = 2 \times$ number of harmonics + 1), the vector \mathcal{J} has now $M = N + 1$ components and T a $N \times M$ matrix.

Letting L be the number of sets of values (x, \mathcal{J}) corresponding to L test points, an $M \times L$ matrix $[X]$ and an $M \times L$ matrix $[\mathcal{J}]$ can be constructed by juxtaposition of the L column vectors x and \mathcal{J} , and Eq. 7 may be written as :

$$[X] = T [\mathcal{J}] \quad (15)$$

When $L = M$, T can be obtained by a simple inversion :

$$T = [X] [\mathcal{J}]^{-1} \quad (16)$$

In such case, if a vector x is computed from a measured \mathcal{J} and the computed τ given by Eq. 16, its value \hat{x} is such that :

$$\hat{x} - x = 0$$

When L is greater than M , there is no solution to Eq. 8 because in general, x and \mathcal{J} do not verify Eq. 14 exactly and Eq. 15 is a system of uncompatible equations. However, a value of τ can be found which minimizes the quantity :

$$Q = \sum_{i=1,L} (\hat{x}_i - x_i)^T (\hat{x}_i - x_i) = \sum_{i=1,L} (\tau \mathcal{J}_i - x_i)^T (\tau \mathcal{J}_i - x_i) \quad (17)$$

(where the upperscript τ denotes a transposition).

Q is the quadratic error between the measured values x and the computed (or "estimated") values \hat{x} . If x and \mathcal{J} verify Eq. 14 and no measurement error is made, Q is zero. Otherwise the value of Q is a measure of the correlation of x and \mathcal{J} with respect to the model. It can be seen indeed, that it would be approximately equivalent to choose M test points, to determine a value of τ with Eq. 16, and then apply Eq. 14 to the $L - M$ remaining test points. Letting :

$$S = \sum_{i=1,L} x_i^T x_i$$

a correlation coefficient can be defined as :

$$C = 1 - \sqrt{\frac{L}{L-M} (Q/S)} \quad (18)$$

Since Q is a quadratic function of the "output" x of the model, its minimization leads to a least square estimate of τ given by :

$$\tau = [X] [\mathcal{J}]^T ([\mathcal{J}] [\mathcal{J}]^T)^{-1} \quad (19)$$

Once τ has been obtained by Eq. 19, the estimated x is computed from the measured \mathcal{J} by Eq. 14 and compared to the measured x for each test point i , in order to obtain :

- the quadratic error

$$Q_i = (\hat{x}_i - x_i)^T (\hat{x}_i - x_i) \quad (20)$$

- the relative error

$$\epsilon_i = \sqrt{Q_i / (x_i^T x_i)} \quad (21)$$

- the averaged error is then defined as

$$\langle \epsilon \rangle = \frac{1}{L} \sum_{i=1,L} \epsilon_i \quad (22)$$

In this case (N - 3) components of σ_m have to be cancelled, and (N - 3) components of δ_m are available which can be therefore uniquely defined by solving Eq. 23. The corresponding multicyclic cam obtained in this case was denoted "A" type cam in Ref. 11.

However, as far as the stresses are concerned, it is usually considered that the important reference parameter is the peak-to-peak value. Therefore it is more appropriate to determine a multicyclic cam which would minimize the peak-to-peak value of the stress. Unfortunately, such an optimization problem cannot be solved analytically, but only on the computer, by iterative algorithms.

As shown in Ref. 11, the optimal "A" cam does not necessarily reduce the peak-to-peak values because the decrease in harmonics 2, 3, ... magnitude may be associated with an increase in harmonic 1 magnitude which will result in an overall increase of the peak-to-peak level. Although not equivalent to a peak-to-peak minimization, the minimization of a quadratic function of all harmonics of the stress would give a closer, and therefore better, solution.

A type "B" ideal cam is defined as minimizing the quantity :

$$Q_m = \sigma_m^T \sigma_m$$

In this case indeed, σ_m contains (N - 1) components and they are only (N - 3) in δ_m . Therefore there is in general no δ_m for which $\sigma_m = 0$.

However it is possible to find a value of δ_m which minimize Q_m , and this value is given by :

$$\delta_{id} = - (T_m^T T_m)^{-1} T_m^T (T_p \delta_p + \sigma_{m0}) \quad (24)$$

This shows that the ideal cam depends upon the rotor control δ_p . When several configurations are considered it is possible to define an averaged value of δ_{id} . This average defines a cam which will have stress reducing effects in all cases, if the term $T_p \delta_p$ does not vary too much from one configuration to another. Such cam is called "optimal" and the "B" type is defined by :

$$\delta_B = - (T_m^T T_m)^{-1} T_m^T (T_p \langle \delta_p \rangle + \sigma_{m0}) \quad (25)$$

where the symbol $\langle \rangle$ denotes an averaged value.

3.4 Fixed stick and fixed flight conditions

Equations 24 and 25 define cams for fixed stick conditions since \mathcal{J}_p is supposed to be unchanged. The stress reduction may be defined by comparing the stress peak-to-peak value when no multicyclic control is applied, with the case where the cam is introduced.

An other possibility should be considered because, as it will be shown later (see paragraph B III), the forces acting on the rotor hub (L, X, Y) depend upon the collective and cyclic pitch, which is well known, but also upon the multicyclic components.

Therefore the introduction of a cam will always modify the equilibrium of the rotor. In a real flight, the imposed conditions are lift, propulsion and lateral force, rather than the 'stick' position (in fact the collective and cyclic controls).

Therefore the control \mathcal{J}_p should be changed to maintain L, X and Y the same.

Because L, X and Y can be also linearly related to the deflection \mathcal{J} (as shown in B III), the stress can be expressed by an equation similar to Eq. 23 :

$$\sigma_m = T_p' \mathcal{J}_p' + T_m' \mathcal{J}_m + \sigma_{m_0}' \quad (26)$$

where \mathcal{J}_p' is a vector of components L, X, Y.

In the same way, the ideal cam for fixed flight conditions is obtained by :

$$(\mathcal{J}_{id})_{FFC} = - (T_m'^T T_m')^{-1} T_m'^T (T_p' \mathcal{J}_p' + \sigma_{m_0}') \quad (27)$$

The method described in paragraph 3.2 readily applies for determining the matrices T_p' , T_m' and the vector σ_{m_0}' which can be casted into a single matrix T' (like T_p , T_m and σ_m in T) while a vector \mathcal{J}' is constructed with L, X, Y as the three first components, the others being the same as those of \mathcal{J} (i. e. multicyclic terms and I.).

It comes then :

$$\sigma = T' \mathcal{J}'$$

and T' is obtained from measurements of σ and \mathcal{J}' by equation 19, which gives in this case :

$$T' = [\sigma] [\mathcal{J}'] [\mathcal{J}' \mathcal{J}'^T]^{-1}$$

4. - IMPROVEMENTS AND EXTENSION OF THE METHOD4.1 Matrix regularity

Since the computation of τ by Eq. 19 requires an inversion, it is important that the matrix $([\delta] \quad [\delta']^T)$ be not only regular but also well-conditioned. Otherwise instability may appear in the coefficients of τ . Ill-conditioning comes from a "linear closeness" between some vectors δ and its detection would in general require special algorithms. (See Ref. 5 for instance). In the present case, linear closeness occurs because the collective value is always close to 24 degrees in all runs, and the last component of δ is already equal to 1 in all runs. To avoid instability, 24 degrees is taken as a reference value for the collective, and it is the difference between the actual collective and this value which is entered as the first component of δ . Also, before inverting the matrix, a quick check is made to eliminate pairs of linearly close vectors or null vectors. In this case some columns of τ are missing since they cannot be determined from the data (this happens indeed with simulated data where cyclic and collective terms are strictly constant).

4.2 Effect of the rotor shaft angle α_s .

Because of the limited number of runs available at constant μ and α_s a correlation analysis on more runs was not possible unless the effect of α_s could be included in the model.

This can be done simply by assuming* that the effect of α_s is independent of δ and can be represented by a vector σ_s such that Eq. 14 is replaced by :

$$\sigma = \tau \delta + \alpha_s \sigma_s \quad (28)$$

By adding to τ an extra component representing σ_s and an extra component to δ equal to α_s , Eq. 14 can still be used and the same method remains valid for determining τ by a least square regression. In this case however :

$$M = N + 2$$

and, in the computation of ideal and optimal cams, σ_{m_0} is to be replaced by :

$$\sigma_{m_0} + \alpha_s \sigma_s$$

* This can be deduced from Eq. 2 since $\alpha_q = \alpha_s + \beta_1$

4.3 Effect of the advance ratio

The variation of the rotor response with the advance ratio, at constant RPM, may be described by the evolution of the matrix T when μ varies.

If T is known for a given value of μ , say μ_0 , a first order expansion of T may be written as

$$T(\mu) = T(\mu_0) + (\mu - \mu_0) T_\mu$$

The matrix T_μ may be identified by the same method as T if the following transformation is made :

$$\sigma' = \sigma(\mu) - T(\mu_0) \delta$$

$$\delta' = (\mu - \mu_0) \delta$$

since

$$\sigma(\mu) = T(\mu) \delta$$

it comes :

$$\sigma' = T_\mu \delta' \quad (29)$$

4.4 Evaluation of the stress reducing effect of the cams

In the present tests, the mechanical cams have been tried with various phase and amplitude settings. As shown in Section C, I, stresses were reduced in some cases, increased in others. To evaluate properly the effect of ideal and optimal cams, stresses are first computed with no multicyclic cam and then compared to those obtained with ideal and optimal cams. If the ideal cam gives the maximum reduction, a slightly different cam would obviously give a little less. To have a measure of the difference between the ideal cam and another (like optimal or real), the following quantity is computed, "relative distance" between the cams in the Fourier space :

$$d = \frac{(\delta_{id} - \delta_m)(\delta_{id} - \delta_m)}{\delta_{id}^T \delta_{id}} \quad (30)$$

where the vectors δ_{id} and δ_m contain respectively the multicyclic components of the ideal and the other cam.

5. - COMPUTER PROGRAM FOR τ MATRIX IDENTIFICATION AND OPTIMAL CAM EVALUATION

A FORTRAN IV program was written originally for the IBM 1130 and then extended for the IBM 360/75.

5.1 Operations performed

This program analyses a maximum of 30 test points given by the Fourier coefficients of the jet-flap deflection and the considered stress, up to the 4th harmonic. It performs the following operations :

- a) Computation of the τ matrix according to Eq. 19,
- b) Computation of the ideal cam for each test point, and of the optimal cam. Type "A" cams were used in a first version of the program and are now replaced by type "B",
- c) For each test point
 - c1 Computation of the Fourier coefficients of the stress in two cases :
 - . from the measured δ ,
 - . from the actual rotor control and the optimal cam.
 - c2 Computation of the quadratic error Q_i and the relative error ϵ_i (from Eq. 20 and 21),
 - c3 Computation and comparison of the peak-to-peak values
 - . measured directly
 - . computed from the real flap deflection
 - . computed from the real δ_p with no cam
 - . computed from the real δ_p and the optimal cam
 - . computed from the real δ_p and the ideal cam
 - c4 Computation of the relative distances to the ideal cam of the real and optimal cams,
 - c5 Computation of the maximum flap deflections obtained with the real δ_p and the optimal cam,
 - c6 Plot of the time histories (e.g. values of the stresses vs. Blade azimuth position) of the measured, computed and optimal stress.
- d) At the end of the program, the relative error $\langle \epsilon \rangle$ and correlation coefficient C.

5.2 General organization of the program

5.2.1 Main program

In the main the principal arrays are dimensionned and the

following input cards are read :

- First card : comments
- Second card : program parameters (number of runs, of harmonics, value of the collective reference)
- Third card : program options (variable α_g , variable μ)
- Next cards : contain the data concerning the runs to be analysed. For each run :
 - . the Fourier coefficients of the stress (or any other quantities which need to be analysed) with eventually the value of μ .
 - . the Fourier coefficients of the jet flap deflection with eventually the value of α_g .

When the μ option is used, an additional set of cards containing the matrix T and the corresponding value of μ should be read.

5.2.2. Subroutine MUTMA (Multicyclic transfer Matrix Analysis)

It constitutes the main core of the program and performs operations a, b, c, and d described previously. Options are available making possible :

- to read in the matrix T (instead of computing it)
- to compute the matrix T only
- to read in an optimal cam
- to perform the analysis without computing ideals and optimal cams.

Several subroutines are used in conjunction with MUTMA performing special operations :

- ARGFI

Computes the amplitude and the position of the first maximum of each harmonic of a cam (given by its sine and cosine coefficients).

- CAM

Computes and stores the ideal and optimal cams.

- MATRA

Computes the transposed of a matrix.

- MINV

Computes the inverse of a matrix (Internal computations are made in a double precision arithmetic).

- PEAK

Computes the values of a function given by its sine and cosine Fourier coefficients, at every five degrees, stores these values (can store 3 functions, e.g. measured, computed and optimal stress), computes the maximum, the minimum, the corresponding values of ψ , and then the peak-to-peak value.

- PLOT

Plot and print the values stored by peak.
A simultaneous plot of three functions is possible.

- PROD

Computes the product of two general matrices.

- SMPI

Check the regularity of a square symmetric matrix and proceed with a partial inversion if dependent or null vectors are found. For instance the matrices

$$\begin{array}{c} \left| \begin{array}{ccc} 0 & a & b \\ 0 & & A \\ 0 & & \end{array} \right| , \left| \begin{array}{ccc} ab & a & 0 \\ a & a/b & 0 \\ 0 & 0 & c \end{array} \right| \end{array} \quad \text{Will give on}$$

return :

$$\left| \begin{array}{ccc} 0 & 0 & 0 \\ 0 & & A^{-1} \\ 0 & & \end{array} \right| , \left| \begin{array}{ccc} 0 & 0 & 0 \\ 0 & b/a & 0 \\ 0 & 0 & 1/c \end{array} \right|$$

The listings of these programs are available at GIRAVIONS DORAND but will not be joined to the present report. However, an example of output will be presented in Appendix I.

5.3 Possibilities of the program

It is worth noting that, due to the particular form of Eq. 19, each component of the vector X, no matter what it does represent (i.e. whether it is actually a Fourier coefficient of a quantity or any other static value) can be separately related to the Fourier components of the flap deflection and α_s (i.e. each line of the matrix τ is evaluated separately).

Therefore this program can be used to correlate different quantities, independent of each other, to the flap deflection. A remarkable application of this possibility has been the correlation of the aerodynamic coefficient C_{LR} , C_{XR} , C_Y , etc. to the δ and α_s as described later in III, 6.

Also, once τ has been determined, it represents completely the rotor (for given μ , θ and Ω).

Thus it is possible to predict the behavior of the rotor for arbitrary flight conditions or cam configuration.

III. -APPLICATION TO THE TEST DATA

1. - JET FLAP DEFLECTION FOURIER ANALYSIS

In order to perform the multicyclic transfer matrix analysis, it is first necessary to know the actual flap deflection Fourier coefficients.

A total of thirty test points have been studied corresponding to the conditions :

$$\mu = 0.4 \quad \Omega = 250 \text{ rpm} \quad \theta_{0.7} = 5^\circ$$

A first analysis was made at GIRAVIONS DORAND using a mechanical Fourier analyser, directly from the oscillograph records. This is not a very precise method, and later on, the harmonic analysis of the same 30 signals was made at NASA, AMES Research Center, using discrete measurements of the oscillograph records and a digital computer processing.

Values of the Fourier coefficients obtained by this method are given in Table VIII, up to the 4th harmonic.

2. - ANALYSIS OF THE FLAP BENDING STRESS

Signals corresponding to the flap bending stress at 0.45 and 0.7R have been first processed at GIRAVIONS DORAND from the original oscillograph records, in order to obtain 60 discrete numerical values per period. These sets of values were then Fourier analysed on the digital computer at AMES.

The Fourier coefficients of the flap bending stress at 0.45 R are given in table IX. Note that three runs were entirely analysed at GIRAVIONS DORAND.

After encouraging results obtained with fewer runs (see ref. 6), the matrix analysis was performed for the 30 runs, first using the G. D. values for the flap deflection, then the NASA values.

The error patterns obtained with G. D. and NASA values are displayed in Fig. 48 where the errors ϵ are sorted by increasing values. They show that a good correlation is obtained in both cases for the 30 runs and that this correlation is increased with increasing precision in the measurements of δ , indicating therefore that the model is correct but measurement errors are responsible for the scatter of the results.

To obtain a better idea of the statistical distribution of the error, the partition function has been plotted for both cases on Fig. 49.

This function, $F(\xi)$, is the ratio of the number of run whose error is less than ξ , to the total number of runs.

3. - CORRECTION OF PHASE ERRORS

Even with the NASA values, some runs still remained with a large error. For example run 16.08 exhibits a 20% error. If one looks at the waveforms of the computed and measured stress, as sketched in Fig. 50, it appears that the shape is almost correctly reproduced except for a phase shift, which in this case would be of about 10 degrees. Because this error seemed of systematic nature, rather than the result of random errors on the computed or measured Fourier coefficients, the oscillograph records were examined carefully and it was soon discovered that the 1p pip, used to define the rotor period, was not regularly spaced but was undergoing random deviations about some average position. On the contrary, the period deduced

from the occurrence of specific features of the signal itself was perfectly regular. This is believed to be the result of some backlash occurring in the slip ring drive.

Since an error of 1 mm corresponds to 6°, and the undetermination on the 1p pip is, in this run of one or two millimeters, it is not surprising that an error of 10° could have been made.

In order to correct these errors, all the results concerning the 30 runs have been systematically examined, and the phase shift estimated from the comparison between measured and computed wave forms. Then the Fourier coefficients of both δ and σ have been modified consequently.

These corrected values are given in Table X for δ and Table XI for σ 0.45. The value of the correction $\Delta\psi$ is indicated in both tables.

4. - FINAL RESULTS FOR JET FLAP DEFLECTION AND FLAP BENDING STRESS

With the values given in Tables X and XI, a matrix analysis has been performed. A very clear improvement of the correlation has been obtained as it appears on Fig. 48 and 49.

It is interesting to compare the results obtained in different cases of study of the stress at 0.45 R, for fixed stick conditions, i.e. the input is only the Fourier coefficients of the jet flap deflection.

Study Conditions	Number of test points	Average error %	Correlation %	
$\alpha_s = \text{cte}$ G.D. values	15	6.1	81.6	
$\alpha_s = \text{variable}$ {	G.D. values	30	9.2	85.5
	NASA values	30	8.9	86
	Phase corrected	30	6.9	89

This shows that the correlation stays almost constant although the number of test points processed is doubled, which is an excellent proof of the statistical validity of the model. The effect of decreasing the measurement error is an increase of the correlation, which is also supporting this model.

4.1 Fixed stick conditions

The analysis of 30 test points from the values given in Tables X and XI leads to a value of the T matrix elements given in Table XII.

Boxes contain the coefficients of one harmonic upon an other one. In order to emphasize the role of the different multicyclic components upon the harmonic content of the stress, each box may be reduced to one value expressing an average ratio of amplitudes. This gives in this case the following matrix.

\mathcal{J}	0p	1p	2p	3p	4p
0p	1.	0.2	0.15	0.13	1.
1p	0.33	0.71	0.08	0.51	0.85
2p	0.41	0.47	1.1	0.34	0.64
3p	0.26	1.1	1.2	3.9	4.37
4p	0.34	1.37	0.72	2.1	5.6

where the coefficients have been normalized to $\sigma_o / \mathcal{J}_o = 0.12$ hbar/degree.

This way of depicting the multicyclic effects is rather qualitative but gives a fair approximation of the influence of the jet flap deflection harmonics. It can be deduced for instance that 1 degree of harmonic 4p in flap deflection will result into $0.85 \times 0.12 = 0.1$ hbar amplitude of harmonic 1p, $0.64 \times 0.12 = 0.072$ hbar amplitude of harmonic 2 p and so on.

These coefficients show also the remarquable increase in efficiency as higher harmonics are concerned, which could be the result of the rotor blades being near a first mode resonance for frequencies corresponding to harmonic 4p.

This is emphasized by plotting the harmonic amplitude of the stress as a function of the rank of the harmonic of \mathcal{J} . In general $\sigma_n = f(\mathcal{J}_n)$ would represent an ordinary linear transfer function. Due to non linearities $\sigma_n = f(\mathcal{J}_p)$ is not zero and may be interpreted as cross transfer functions. These curves are displayed in Fig. 51.

In fig. 52 are represented the stress harmonic sensitivity to rotor shaft angle α_1 and flap deflection harmonics. The numerical results of the analysis are given in Table XIII. As mentioned previously the correlation obtained is fairly good, the average error being of 6.9%.

The different ideal "B" cams and the optimal cam corresponding to those 30 runs are sketched on Fig. 53. It is remarkable to note that the phase dispersion is small for the ideal cams, but amplitude may be quite different. The dispersion in the ideal cams comes from the different values of the control δ_P and angle α_S according to Eq. 24.

If $T_P \delta_P$ is not varying too much compared to $(\sigma_{m_0} + \alpha_S \sigma_S)$, then the dispersion is small.

The optimal cam found in this case is the following :

$$\delta_{opt} = 3.9 \cos 2\psi - 1.1 \sin 2\psi - 3.1 \cos 3\psi - 0.1 \sin 3\psi - 2. \cos 4\psi - 0.9 \sin 4\psi.$$

In Fig. 54 are plotted the stress reduction obtained with the optimal "B" cam and the real cam (normalized to the ideal "B" cam reduction), versus the "relative distance" defined by Eq. 30. When this distance is small, the reduction obtained becomes comparable to the ideal reduction. However, since the ideal cam does not exactly minimize the peak-to-peak values in some instances the optimal cam could give better results, than expected. Nevertheless the general pattern indicates that the quadratic criterion is a good approximation for rapid investigations. If a type "C" cam is defined as the cam minimizing the peak-to-peak, type "B" could be used as a starting point in an optimization algorithm for determining the "C" cam.

4.2 Fixed flight conditions

The results concerning the fixed flight conditions are of course of greater interest since it corresponds more closely to the real helicopter case.

To run this analysis, the values of δ_0 , δ_1 and δ_1' have been replaced respectively by those of C_{LR}/G , C_{XR}/G and C_Y/G extracted from Table II.

(In fact, these three coefficients have been multiplied by a factor 10^3 in order to have reasonable coefficients in the matrix T).

The corresponding matrix T found in this case is given in Table XIV. It differs from the matrix obtained in fixed stick conditions because of the influence of the multicyclic flap deflection upon the values of C_L , C_x and C_y . As will be seen in paragraph 6,

$$\delta_P' = \begin{vmatrix} C_{LR}/G \\ C_{XR}/G \\ C_Y/G \end{vmatrix} = F_P \delta_P + F_m \delta_m + F_{m_0}$$

Eq. 26 gives then

$$\sigma_m = (T_P' F_P) \delta_P + (T_P' F_m + T_m') \delta_m + (T_P' F_{m_0} + \sigma_{m_0}')$$

comparing to Eq. 23 it comes :

$$T_P = T_P' F_P$$

$$T_m = T_m' + T_P' F_m$$

However it seems that the term $T_P' F_m$ is not very important as attested by the similarity between T_m and T_m' (e.g. see Tables XII and XIV).

Results concerning the analysis of the 30 runs are given in Table XV and deserve some comments.

Although the error is 2% higher than in the fixed stick case (due, it seems, to some errors in the measurements of C_{LR} , C_{XR} and C_Y), the match between the model and the data is still good.

The reductions obtained with the ideal cam reach values as high as 66% and is never less than 40%. The averaged reduction is 49%.

With the optimal cam, an average reduction of the stress of 36% is found.

These results seem to agree very well with the reductions observed experimentally.

Ideal and optimal cams are sketched in Fig. 55, exhibiting the same concentration of the phases.

On Fig. 56, the optimal cam is compared with the experimental cam IV.

Except for the 2p harmonic, there is a remarkable similarity between these two cams.

The optimal cam for fixed flight conditions is given analytically by (fig. 62) :

$$\delta_{opt} = 3.4 \cos 2\psi + 1.4 \sin 2\psi - 5.7 \cos 3\psi - 4.5 \sin 3\psi - 7.5 \cos 4\psi - 4.8 \sin 4\psi.$$

It is worth noting that the harmonics amplitude though greater than in the fixed stick conditions, are still reasonable and could be actually obtained on the jet flap.

5. - ANALYSIS OF THE VIBRATIONS

5.1 Introduction

The method used successfully for the analysis of the flap bending stresses can be equally well applied to the problem of the vibratory forces on the rotor hub.

Reduction of these vibrations are indeed a major problem in helicopter technology and the multicyclic control of the rotor appears to be a very powerful mean of controlling these vibrations, as already seen in Section B, I.

The forces and moments acting on the rotor hub were measured by a 6 - component balance. The forces on the three vertical arms of the balance correspond to the signals recorded by the galvanometers 5.1 (left aft arm), 5.2 (right aft arm), 5.3 (forward arm).

The sum of these signals gives the vertical force acting on the hub. The variations of this force define the vertical vibrations induced by the rotor, which will be transmitted to the fuselage in case of a real helicopter.

5.2 Processing of the test data

The Fourier coefficients of the vibratory forces have been obtained from the oscillograph records using a mechanical Fourier analyser. The value of the coefficient is read on the instrument in millimeters, with an error of ± 0.05 mm. This corresponds to an error of ± 2 daN in the recordings considered here. In fact, because of the difficulty of following exactly the waveform, the error is about ± 6 daN.

The coefficients for the vibratory force F_z have been finally obtained by summing up of the signals 5.1, 5.2 and 5.3.

Because of the amount of time required, the analysis has been limited :

- to the even harmonics (0, P2 and P4), since the odd ones should normally cancel out in a two-bladed rotor, if non-symmetrical effects are not present.
- to the minimum number of runs needed to obtain a matrix T.

For this second condition, 11 runs are necessary when the option is used and 4 harmonics considered.

Using the dependency analysis described in Ref.10, 11 vectors \mathcal{J} have been chosen among the 30 considered in the analysis of the stresses in order to obtain a basis as orthogonal as possible. A twelfth run was added to these to evaluate the correlation.

In Table XVI are given the Fourier coefficients, for these 12 runs, of the signals 5.1, 5.2, 5.3 and the resultant vibratory force F_z .

5.3 Analysis of the vibratory force

When the multicyclic transfer matrix analysis is applied to the vibratory forces, a particular problem appears due to the fact that harmonics 1p and 3p are absent. The matrix T has thus four rows of zeros as can be seen in table XVII (fixed stick conditions, f. s. c.) and table XVIII (fixed flight conditions, f. f. c)

In this case the matrix $(T_m^T T_m)$ of Eq. (24) is irregular and the program normally fails when computing the ideal cams. The physical reason for this is that there are four quantities to define the vibrations (f_2, f_2', f_4, f_4') , but six variables to adjust in the flap deflection $(\mathcal{J}_2^f, \mathcal{J}_2^g, \mathcal{J}_3^f, \mathcal{J}_3^g, \mathcal{J}_4^f, \mathcal{J}_4^g)$ in order to minimize the vibration.

The problem is therefore undetermined. It is possible, however, to solve this by deciding not to consider harmonic 3p in the multicyclic cam. In this case, the vibration may be exactly cancelled out since its four Fourier coefficients are linearly related to the four Fourier coefficients of the cam. -

A slight modification of the program "CAM" is necessary to compute the ideal cams.

Its consists in setting to zero, the columns of T_m corresponding to harmonic 3p. In this case the subroutine SMPI will recognize corresponding zeros in $(T_m^T T_m)$ and proceed with the inversion of the reduced matrix without any problem.

Ideal and optimal cams are plotted in figure 57 for fixed stick conditions and figure 58 for fixed flight conditions. It should be noted that the dispersion among the ideal cams is of the same order as for the stress cams.

In tables XIX and XX are given the results of the analysis for fixed stick and fixed flight conditions. The correlation is very good.

The vibration reduction by the ideal cam is always 100% but the optimal cam gives an averaged reduction of 40% (for f. s. c.) and 29% (for f. f. c.) which shows that the same type of cam could be used in all flight conditions (with $\mu = 0.4$).

The optimal cams for vibrations are given by :

f. s. c.

$$\delta_{opt} = 24.1 \cos 2\psi - 0.6 \sin 2\psi + 7.2 \cos 4\psi + 11.9 \sin 4\psi$$

f. f. c.

$$\delta_{opt} = -5.2 \cos 2\psi - 8.2 \sin 2\psi + 2.5 \cos 4\psi + 1.1 \sin 4\psi$$

It is interesting to note the difference with the cam obtained for reducing the stresses. Also these cams may be compared to the optimal cam obtained in the simulations analysed in paragraph II 1 and II 2.2. These simulations give the coefficients of C_T , which is closely related to the vibrations. The cam obtained in this case (for fixed stick conditions) is :

$$\delta_{opt} = -13.2 \cos 2\psi - 2.8 \sin 2\psi + 0.3 \cos 3\psi + 2. \sin 3\psi$$

and reduction obtained was 64%.

Harmonic 3p was considered here because non-symmetric effects were considered. In figure 59 are compared the simulation and real test optimal cams.

Finally, in figure 60 and 61 are represented the transfer functions and harmonic sensitivity as was done previously for the stresses, showing the influence of the flap bending mode resonance.

6. - ANALYSIS OF THE AERODYNAMIC COEFFICIENTS

6.1 Matrix T

It is possible to apply the matrix analysis to correlate some aerodynamic coefficients to the flap deflection and rotor shaft angle α_3 .

The same program is used, but the aerodynamic coefficients are introduced instead of the Fourier coefficients of the stresses (or vibrations).

In this case each row of the matrix T gives the derivatives of the corresponding coefficient with respect to δ and α_3 .

The coefficients which have been analysed are :

C_{LR} / G	rotor lift coefficient
C_{XR} / G	rotor propulsive force coefficient
C_Y / G	lateral force coefficient
C_M / G	pitching moment coefficient
C_{RR} / G	rolling moment coefficient

As before, the same 30 runs have been studied.

The corresponding matrix T is given in table XXI.

The influence of multicyclic inputs is quite remarkable especially concerning the 3p and 4p components.

Contribution to lift of these terms is important. For instance, the optimal cam (for fixed flight condition) for reducing the stresses, contributes to about 20% of the lift.

6.2 Flight control matrices

Besides the role of the multicyclic components which is still difficult to explain, it is interesting to know the conventional control effects on the rotor forces.

- The constant term in the C_{LR}/σ coefficients comes from the blade pitch angle $\theta_{0.7}$ which provides a lift even for no flap deflection. By construction of the blade, the lift is zero when $\theta_{0.7} = -4^\circ$.

It comes therefore :

$$10^3 C_{LR}/\sigma = 3.3 \delta_0 + 0.2 \delta_1' + 12. (\theta_{0.7} + 4) + 8.1 \alpha_s$$

- For the propulsion :

$$10^3 C_{XR}/\sigma = 0.2 \delta_0 + 0.2 \delta_1 - 0.4 \delta_1' - 11.3 - 1.2 \alpha_s$$

Here the value - 11.3 represents the drag of the rotor. It is interesting to note that for $\alpha_s = -10^\circ$, this drag is just balanced by the rotor tilt.

- For the lateral forces :

$$10^3 C_Y/\sigma = 0.3 \delta_0 - 0.3 \delta_1 + 0.1 \delta_1' - 0.9 + 0.4 \alpha_s$$

The value - 0.9 indicates that the rotor tends normally to tilt to the left (when facing the wind). This increase markedly when the rotor shaft is tilted forward.

From the three preceding equations one can deduce the controls to be applied to the rotor in order to obtain given forces :

$$\begin{cases} \delta_0 = 2.67 (10^3 C_{LR}/\sigma - 107.8) + 0.248 (10^3 C_{XR}/\sigma + 11.3) + 0.18 (10^3 C_Y/\sigma + 0.9) - 21.4 \alpha_s \\ \delta_1 = 0.585 (10^3 C_{LR}/\sigma - 107.8) - 1.42 (10^3 C_{XR}/\sigma + 11.3) - 4.9 (10^3 C_Y/\sigma + 0.9) - 4.5 \alpha_s \\ \delta_1' = 0.48 (10^3 C_{LR}/\sigma - 107.8) - 3.27 (10^3 C_{XR}/\sigma + 11.3) - 2.39 (10^3 C_Y/\sigma - 0.9) - 6.8 \alpha_s \end{cases}$$

(It is to be recalled that these coefficients are only valid for $\mu = 0.4$, $\theta_{0.7} = 5^\circ$ and $\Omega = 250$ r.p.m.).

6.3 Analysis of Performance characteristics

The domain of the tests, presented in tables I.1 through I.23, comprises 29 runs and 334 test points performed at wind tunnel speeds ranging from 0 to 123 knots, highest speed attained (see figure 63). These basic data has been processed by standard computer techniques, tables II.1 through II.24.

The results obtained have been presented graphically, see figures 1 through 20.

The tests have been focused on comparatively high tip-speed ratios attaining 0.7. However, neither maximum nor optimum capabilities of the jet-flap rotor could be demonstrated during this series of tests because of lack of power of the compressed air supply generator. The comparison with the first series of tests shows that the performance remains unchanged since the modifications introduced in 1965, fig. 1a. The test domain has been enlarged to very high blade loadings, the highest \bar{C}_L recorded in hover configuration reached 3.26 for a ratio of C_{LR}/C_{JR} of 4.25. The highest C_{LR}/C_{JR} ratio, which is comparable with the L/D ratio, is 6.5 at C_L equal to 1.07. At advance ratio 0.25 we have $C_{LR}/C_{JR} = 6.1$ at $\bar{C}_L = 1.05$. With increased tip-speed ratios these characteristics are somewhat lower, at $V/\Omega R = 0.6$, $C_{LR}/C_{JR} = 5.1$ at $\bar{C}_L = 0.97$. At the same time high propulsion forces are maintained at forward flight. At advance ratio of 0.6 the ratio X/L is still 12.4%. As we mentioned these characteristics are neither the highest possible nor the optimal. A better power adaptation would permit a much more effective demonstration of jet-flap rotor capabilities.

As seen in the figures 1 to 20 a high degree of scatter existed during these tests. In fact difficulties were encountered to maintain all but one parameter constant during the tests. In particular, secondary effects such as multicyclic effects have been present in most tests. It would be useful to employ a more advanced technique of analysis to obtain more consistent results. Such an approach has been outlined above but has not been pursued much further because of limited time allotted to the present analysis.

CONCLUSIONS1. DATA PROCESSING

The 1971 tests of the Dorand H-2011 rotor have been analyzed to answer the following two main themes of research :

- a) Effectiveness of multicyclic effects on the reduction of stresses and vibrations at high advance ratios.
- b) Influence of minor modifications which the rotor has undergone since the previous tests, in 1965, on the general performance characteristics.

On the outset of the data processing work it became obvious that a special analytical procedure was necessary to obtain a clear picture of the multicyclic phenomena we encountered in the experimentation domain covering some 300 test points and μ values ranging from 0.25 to 0.70. Such a procedure has been established and has permitted to deal with the total experimental data output in what can be considered a simple and global manner. The basic idea behind the procedure used consists in relating the output values, stresses or vibratory forces, to input signals, multicyclic jet deflections, by a transfer matrix. Analytical and experimental work has shown that such transfer matrices exist and are practically invariant for given advance ratio. This procedure, it is believed, opens a very wide field of investigation to most rotary wing problems concerning stresses and vibrations.

The existence of a unique matrix representing the transfer of control inputs to measured stress and vibratory forces has permitted to optimize the multicyclic components to obtain maximum stress or vibration reductions. The tests have already shown reductions reaching 50% of stress or vibration levels. These reductions have been obtained by a sweeping method. A more systematic approach during the first series of tests has not been possible for the following reasons :

- 1) The data obtained could not be analysed instantaneously.
- 2) No simple method existed to guide the choice of multicyclic laws to obtain better reductions of stresses and vibrations.

- 3) The correlation between the control inputs and multicyclic effects of the jet flap was comparatively poor, because of mechanical wear and backlash in control linkages progressing rapidly with number of runs.

2. VIBRATORY STRESS ANALYSIS

The stresses measured at 0.45 and 0.70R have been recorded and Fourier analyzed for 30 test points at μ 0.4. Because of near resonance conditions the results show a strong effectiveness of 3 P and 4 P signals e.g. a 4 P jet flap input results in a 4 P stress 5.1 times higher than 2 P stress resulting from a 2 P jet flap input. The interharmonic couplings appear very strong. The analysis has shown that stress harmonics higher than 5P can be neglected. The sensitivity to the jet flap deflections varied from 0.10 hbar per degree of jet flap deflection for 1 P and 2 P to 0.48 for 3 P and 4 P control inputs. Similar trends are shown in the study of the bending stress sensitivity to the rotor shaft angle. The correlation obtained is fairly good, the average error being 6.9%.

Though the tests have been done in "fixed stick conditions", the "fixed flight conditions" which are of greater interest as they correspond more closely to the real helicopter case, have been investigated. The stress reductions obtained with "ideal cam" reach values as high as 66% and never less than 40%. In both cases the match between the matrix model and the data is good, though the error is 2% higher for the fixed flight conditions.

The computational difficulties to use the peak-to-peak level as an optimization criterium have necessitated the introduction of multicyclic laws ("ideal" cams and "optimal" cams) reducing in some quadric sense the harmonic content, but not necessarily the general peak-to-peak value. It was remarkable to find that the ideal and optimal cams exhibit the same phase characteristics. Moreover, when compared with the optimal cam, the experimental cam N° IV shows a noticeable similarity except for the 2 P harmonic.

The optimal cam for fixed flight conditions is given analytically by :

$$\delta_{opt} = 3.4 \cos 2 \psi - 5.7 \cos 3 \psi - 7.5 \cos 4 \psi \\ + 1.4 \sin 2 \psi - 4.5 \sin 3 \psi - 4.8 \sin 4 \psi,$$

δ_{opt} being expressed in degrees of jet flap deflection.

3. VIBRATORY FORCES

The vibratory forces on the rotor have been measured by load cells situated beneath the hub and Fourier analyzed. Only vertical forces of 0, 2P and 4P components have been taken into account. The same matrix method has been used for analysis of the bending stresses with the modification cancelling the 3P δ components. However, to eliminate the undetermination stemming from the fact that the flap deflection was defined by six variables and the vibrations by four only, the analysis used 12 test points to evaluate the transfer matrix.

The highest vibration reduction noted experimentally was 48% (run 25.2 and 25.5). Analytically defined optimal cam laws differ for fixed stick and fixed flight conditions. In general the multicyclic effects which are optimal for stress reductions are not the same as for vibration reductions.

The limited scope of work has not permitted to obtain a clear understanding of phenomena which govern the optimization of multicyclic laws. It is believed that a considerable research effort is necessary to define the cause - effect links and the sensitivities to various rotor parameters. It is also suggested to improve the investigation techniques and replace mechanical cams by electro-hydraulic devices which are more flexible in obtaining desired multicyclic laws.

At $\mu = 0.4$ and for fixed stick conditions the optimal cam for vibration reductions gives an averaged reduction of 40%. The multicyclic law of the cam expressed in degrees of jet flap deflection is as follows :

$$\delta_{opt} = 24.1 \cos 2 \psi - 0.6 \sin 2 \psi + 7.2 \cos 4 \psi + 11.9 \sin 4 \psi$$

Introduction of non-symmetric effects seems to improve the results. When based on dynamically variable C_T coefficient, which is closely related to vibrations on the hub, the reduction obtained was 64%.

4. PERFORMANCE AND AERODYNAMIC ASPECTS OF THE ROTOR

As already shown during the whirl tests outside the tunnel the modifications introduced since the 1965 tests had little influence on the performance of the rotor. The C_{LR}/σ against C_{JR}/σ curve remained unchanged. The only noticeable

change that the modification (which consisted in the increase of the nozzle height from 4.2 mm to 5.3 mm and in the increase of the jet flap deflections from $\pm 25^\circ$ to $\pm 50^\circ$) have brought, was the shift of the zero lift chord, -4.0 degree nose down.

Most of the tests have been performed below the optimal power conditions corresponding to the pressure ratio of 4.0. In fact due to the power supply deficiencies the maximum pressure ratio obtained during the test did not exceed 3.6. The rotor nevertheless produced very high lift and propulsive forces. The highest mean lift coefficient, \bar{C}_L , attained on the blades was 3.2. At advance ratio of 0.6 the propulsion force was still 10% of the lift for $\alpha_s = 12^\circ$. The mean lift coefficient was 1.3. These figures are typical to the jet flap rotor.

An attempt was made to correlate the aerodynamic coefficients to the flap deflections and the rotor shaft angle. The influence of the multicyclic inputs is quite remarkable. For instance the optimal multicyclic law for stress reduction contributes to about 20% of the total lift.

5. FINAL REMARKS

The main conclusions of the work done can be stated as follows :

- 1) The multicyclic effects bear a very strong correlation to the stress levels and vibratory forces.
- 2) The reduction of stresses and vibrations obtained by non optimized test procedures has reached 50% at advance ratio 0.4 (Maximum stress and vibration reductions did not, however, occur at the same multicyclic settings).
- 3) The performance characteristics of the rotor do not seem to be essentially modified by the multicyclic inputs, their contribution may, however, amount to as high as 20% of the total lift (This effect seems to be due to compensation of cyclic inputs by multicyclic inputs in flight fixed condition and has been noted in the domain far from the stall limitations).

- 4) New method of analysis of multicyclic effects has permitted optimization of control inputs. This method is based on transfer matrices, which are practically invariant with blade angle setting, shaft angle, and basic control settings for a given advance ratio. The transfer matrices indicate that, at advance ratio 0.4, for example, stress and vibration reductions of 80% are feasible.
- 5) The modifications introduced to the jet flaps since 1965 tests did not influence the performance of the rotor to a noticeable degree.

The limited scope of the test analysis did not permit to draw definite conclusions concerning the maximum attainable efficiency of the jet flap rotor. However, farther improvements reaching 80% reduction of stresses and vibration are theoretically feasible.

The matrix analysis used to correlate dynamic outputs to multicyclic inputs has been of great help in gaining an initial understanding of the complex relationships between the aeroelastic and aerodynamic phenomena. The work done has lead to the discovery of the existence of a transfer matrix that is invariable under many rotor configuration variations and describes in a most global and simple way the behavior of the rotor in forward flight. It is believed that this new approach to the analysis of the rotary wing phenomena can make a decisive step in solving the inextricable complexity of the mathematical modeling of the helicopter rotors working conditions in most flight configurations.

- 1 "July 1964 Whirl Tests of the DH 2011 Jet Flap Rotor"
Doc. DH 2011-F3 - Vol. I and II March 1965
- 2 "July 1965 Wind Tunnel Tests of the DH 2011 Jet Flap Rotor"
Doc. DH 2011 - 07 - 2197 PH 3/2 May 1966
- 3 Technical Notes Concerning April and October 1969 Whirl Tests of the DH 2011 Jet Flap Rotor
Doc. DH 2011-D NT 47, 48, 49, 50, 51, 52, 60 Apr. -Oct.1969
- 4 "Analytical Investigation of a Helicopter Rotor Driven and Controlled by a Jet Flap"
William T. EVANS and John L. Mc CLOUD III
Doc. NASA TN D 3028 Sept. 1965
- 5 "Performance Characteristics of a Jet Flap Rotor"
Conference on V/STOL Aircraft
NASA Ames Research Center
Mc CLOUD J. L. and EVANS W. T. April 1966
- 6 "Studies of a Large-Scale Jet Flap Rotor in the 40 - by 80 Foot Wind Tunnel "
AHS Symposium Philadelphia Oct. 1972
John L. Mc CLOUD III Oct. 1972
- 7 "Fields of Application of Jet Flapped Rotors"
AGARD Conference Proceedings N° 121
M. KRETZ Sept. 1971
- 8 "Wind - Tunnel Test Program of the DH 2011 Rotor"
Doc. DH 2011-D NT 54 Sept. 1969
- 9 "Representation of Multicyclic Effects by a Linear Transformation "
Doc. DH 2011-D NT 76 July 1971
- 10 "Non Linear Systems Identification in Presence of Non-uniqueness"
J. -N. AUBRUN
Doc. NASA TN D 6467 August 1971
- 11 "Research of a Correlation between Dynamic Stresses in the Blades and the Multicyclic Jet Flap Deflections"
Doc. DH 2011-D NT 80 May 1972

DESCRIPTION OF THE COMPUTER PROGRAM OUTPUTS

In this appendix is given an example of the results of the analysis by transfer matrix program.

This example has been taken from the analysis of the flap-bending stresses at 0.45 R. Thirty runs have been analysed ; the multicyclic cams are computed for fixed stick conditions.

The results corresponding to one test point are given on two sheets of machine paper (tables XXII and XXIII).

1. FIRST SHEET (see table XXII)

- 1.1 Title and test point number : in our example stresses for the run number 14 - 13.
- 1.2 α_s value (here $\alpha_s = - 10$ degrees)
- 1.3 Four columns containing Fourier coefficients (OP, 1P cosine, 1P sine, 2P cosine, etc.) of the optimal, computed and measured stresses and of the difference between computed and measured stresses.

Units for these values are given in the table (here hectobars).

- 1.4 Then is given, the value of the correlation, the quadratic error and the relative error (5.1%).
- 1.5 The following table indicates, for the computed, measured and optimal stresses, the value and the azimuthal location of the maximum and minimum of these functions. It gives also the peak-to-peak value.
- 1.6 After that, for four multicyclic inputs (i.e. no cam, real cam, optimal cam and ideal cam) are computed the following quantities :
 - a)- The relative distance to the ideal cam which by definition equal 0. , for the ideal cam and 1. for the "no cam" case.
 - b)- The peak-to-peak stress reduction (or increase when negative) with respect to the peak-to-peak value when no cam is used.
 - c)- The corresponding peak-to-peak value.
- 1.7 Then is given the maximum and minimum of the jet flap deflection for the optimal cam and their blade azimuthal locations.

2. SECOND SHEET (see table XXIII)

On this sheet are plotted the time histories of the optimal stress (.), computed stress (*) and measured stress (+).

The stresses values for these points are written on the right part of the sheet.

It can be noted that a priority has been established between the symbols * , + and . on the plot,

- if * and + (or .) are at the same place, * is printed,
- if + and . are at the same place, + is printed.

Nevertheless, when this happens, there is no ambiguity about the location of these points because the three corresponding values are known.

Similar outputs are obtained for each test point analysed, but we must remark that the program gives first the matrix T, the Fourier components of the ideal cams and optimal cam.